Sains Malaysiana 53(2)(2024): 347-358
http://doi.org/10.17576/jsm-2024-5302-09

Advance Heteroatom Dopants Nitrogen, Boron, Sulphur, and Phosphorus on Carbon Dots towards Histamine Detection in Fish Sample

(Nitrogen Dopan Heteroatom, Boron, Sulfur dan Fosforus Termaju pada Titik Karbon ke arah Pengesanan Histamin dalam Sampel Ikan)

MOCHAMAD ZAKKI FAHMI[1,2,*], SITI FEBTRIA ASRINI SUGITO[1], NADIA AULIA HANIFAH[1], UMMI LATHIFAH NUR'AINI[1], BAMBANG PURWANTO[3] & LEE HWEI VOON[4]

[1]Department of Chemistry, Universitas Airlangga, Surabaya 60115, Indonesia
[2]Supramodification Nano-micro Engineering Research Group, Universitas Airlangga, Surabaya 60115, Indonesia
[3]Department of Physiology, Universitas Airlangga, Surabaya 60115, Indonesia
[4]Nanotechnology Catalysis Research Centre, University of Malaya, 50603 Kuala Lumpur, Malaysia

Received: 7 August 2023/Accepted: 23 January 2024

ABSTRACT

This study introduces heteroatom-doped carbon dots (CDs), namely boron-sulphur (BS-CDs) and nitrogen-phosphorus (NP-CDs), highlighting their potential as optical materials for sensitive histamine detection in sensor applications. Synthesized through facile pyrolysis of citric acid cores with non-metal dopants, resulting in confirmed graphene-like structures and uniform spheres with crystal diameters below 3 nm of BS-CDs and NP-CDs. The optical properties exhibited blue fluorescence, with emission wavelengths of 280 nm (QY 0.08%) and 420 nm (QY 1.72%) for BS-CDs and NP-CDs, respectively. Despite declined fluorescence intensities due to interfering components, both CDs demonstrated low selectivity for histamine, which increased the intensity in its presence. Notably, BS-CDs exhibited superior detectability of histamine at a low concentration of 26.3 ppm compared to 42.8 ppm for NP-CDs. Cytotoxicity studies indicated low toxicity for both CDs, positioning them as promising candidates for further development as histamine detectors

Keywords: Boron; carbon dots; co-dopants; histamine detector; nitrogen; phosphorus; sulphur

ABSTRAK

Kajian ini memperkenalkan titik karbon terdop heteroatom (CD), iaitu boron-sulfur (BS-CD) dan nitrogen-fosforus (NP-CD), menonjolkan potensinya sebagai bahan optik untuk pengesanan histamin sensitif dalam aplikasi sensor. Disintesis melalui pirolisis mudah teras asid sitrik dengan dopan bukan logam, menghasilkan struktur seperti grafin yang disahkan dan sfera seragam dengan diameter kristal di bawah 3 nm BS-CD dan NP-CD. Sifat optik mengeluarkan pendarfluor biru, dengan panjang gelombang pelepasan 280 nm (QY 0.08%) dan 420 nm (QY 1.72%) masing-masing untuk BS-CD dan NP-CD. Walaupun keamatan pendarfluor menurun disebabkan oleh komponen yang mengganggu, kedua-dua CD menunjukkan selektiviti rendah untuk histamin, yang meningkatkan keamatan dengan kehadirannya. Paling terutama, BS-CD menunjukkan pengesanan histamin yang unggul pada kepekatan rendah 26.3 ppm berbanding 42.8 ppm untuk NP-CD. Kajian sitotoksisiti menunjukkan ketoksikan yang rendah untuk kedua-dua CD, meletakkannya sebagai calon yang berpotensi untuk pembangunan selanjutnya sebagai pengesan histamin.

Kata kunci: Boron; Co-dopan; fosforus; nitrogen; pengesan histamin; sulfur; titik karbon

INTRODUCTION

The agricultural sector dominates the abundance of marine resources, as evidenced by the catch of marine products. A scombroid family is a fish group that is processed and consumed as daily food. This fish has a high level of histamine which comes from the decarboxylase of histidine (Bi et al. 2020). Micro-bacteria cannot obtain at low temperatures; if a decarboxylase

enzyme is formed, the enzyme still produces the histamine even if the micro-bacteria is inactive. A low temperature that reaches the freezing point can activate the role of the decarboxylase enzyme. Formed histamine in fish is hard to remove even it is heated or frozen due to its excellent stability (Bi et al. 2020). Histamine is a biogenic amine formed by the presence of decarboxylase enzymes upon reaching the optimum temperature of 250 °C. Too high histamine content in consumed fish can lead to poisoning. The Food and Drug Administration (FDA) has set the maximum limit for histamine in edible fish at 50 ppm, while the European Union has set it at 100 ppm. Fish toxicity can increase when external microorganisms penetrate the meat of the fish and spoil the fish. Microbes that reduce fish quality, accelerate spoilage, and increase histamine levels include *Bacillus subsites, M. morganii,* and *E. coli* (Bi et al. 2020; DeBeer et al. 2021; Huang et al. 2017).

One of the nanoparticles used as candidates for detecting histamine levels in fish is CDs-based nanoparticles. CDs have unique optical properties with narrow and symmetrical bands used as probes for sensing applications (Yadav et al. 2019). CDs were chosen as a candidate for histamine detection because they have flexible optical properties to adjust the size of the domain and good photostability (Kim & Chang 2016). CDs have low toxicity, excellent photoluminescence (PL) intensity, and good biocompatibility (size, surface finish, and composition). The electronic properties of fluorescent CDs dyes are superior to other fluorescent dyes (Zhang et al. 2020). Structures composed of CDs are stable when dispersed in water and more stable when dispersed in light (Toloza et al. 2017). The synthesis of CDs at high temperatures typically utilizes citric acid, ascorbic acid, amino acids, glucose, and glycerol as the primary precursor (Wang et al. 2016).

CDs can be synthesized using top-down and bottom-up approaches. A bottom-up approach has advantages over a top-down such as having a uniform size and shape (Baker & Baker 2010). There are several types of bottom-up approaches, such as pyrolysis, microwave, coprecipitation, ultrasonication, and sol-gel (Arole & Munde 2014). Pyrolysis is the decomposition process of materials using high temperatures with no air involved during the heating process. It involves carbonizing precursors at high temperatures (Hola et al. 2014; Zuo et al. 2016). Parameters of the pyrolysis method include the reactor system, heating temperature, pressure, presence of the catalyst, and heating time. These parameters influence the composition and final product (Wang & Hu 2014).

Citric acid is used as a carbon source precursor in CDs synthesis. Based on previous research, citric acid exhibits strong emission at 440 nm and possesses optical properties that dominate the spectrum with a high quantum yield (QY) of 52% (Schneider et al. 2017). High QY indicates high solubility in water, excellent monodisperse stability, and solid blue photoluminescence. In addition, citric acid has many advantages, such as being cheap, environmentally friendly, highly biocompatible, and less toxic in healthy cells (Mandawala et al. 2017; Zhou et al. 2015). Fluorescence can be increased by doping with B, S, P, or N atoms. Doping of CDs affects the electron transfer properties and increases the QY, and causes changes in the electronic structure of carbon that form type-n (extra electron) and type-p (extra hole) carriers (Zang et al. 2017; Zhang et al. 2020). Another research explained that doping could enhance selectivity because the dopant adapted bandgap and electron density to the analyzed target (Li, Yu & You 2015).

Due to their remarkable properties, CDs have gained significant attention in various fields. Notably, CDs are versatile biosensor carriers facilitated by their surface modification and water solubility flexibility (Wang et al. 2022). Recent research has aimed to enhance CD functionality through heteroatom doping (nitrogen, boron, sulfur, phosphorus) and surface functionalization. Heteroatom doping can significantly increase the quantum yield (QY) of CDots. Munusamy et al. (2023) produced nitrogen-doped CDs for various sensor applications. Other studies have explored using phosphorus-doped carbon quantum dots (P-CQDs) for detecting ions, such as Cu^{2+}, with high sensitivity and a low detection limit (Preethi, Viswanathan & Ponpandian 2022). Moreover, Chatterjee et al. (2022) successfully developed boron-doped graphene quantum dots anchored to carbon nanotubes, serving as noble metal-free electrocatalysts for uric acid in a wearable sweat sensor. The research conducted by Mirsadoughi et al. (2022) demonstrated the successful use of sulfur-doped CDs to inhibit the FRET mechanism for analyzing cysteine in human blood serum. Gunjal et al. (2023) highlighted that doping heteroatoms into CDs improves their physicochemical properties, visible light absorption probability, and quantum yield, thereby controlling their size, morphology, structure, and band-gap energy, particularly in applications involving sensing through fluorescent and electrochemical techniques.

Boron is an effective dopant doped to CDs through covalent bonding. Boron doping of CDs (B-CDS) can

improve their non-linear optical properties compared to CDs (Bourlinos et al. 2015). Sulphur doping of CDs (S-CDs) significantly increases the quantum yield (QY), reaching 25%, with an average size of 1.1 nm. Another advantage is their high stability, low toxicity, and excellent biocompatibility. S-CDs can also enhance the kinetics of electron transfer and coordination interactions. In addition, s-CDs exhibit high sensitivity, selectivity, and discharge stability in the alkaline pH range (Xu et al. 2015). Adding heteroatom dopants, such as nitrogen or phosphorus, also enhances the CDs selectivity to histamine, as the dopant can enhance the QY and effectively adjust the bandgap and electron density (Toloza et al. 2017). The source of nitrogen (N) dopant is nitric acid (HNO_3), while phosphorus (P) is from phosphoric acid (H_3PO_4) (Ternero-Hidalgo et al. 2016). Doping nitrogen has the advantage of good photostability, whereas it has the weakness of being unable to survive against metal, acid, or base ions. Because of these weaknesses, doping phosphorus mixtures are used as balances. Nitrogen and phosphorus doping CDs (NP-CDs) can enhance water dispersion and high sensitivity even at low concentrations. Selectivity studies are required to identify the effects of the metallic matrix or mineral salts of histamine detection that may be consumed and accumulated in the fish. The presence of inorganic salts can minimize the photoluminescence of the electron transfer process (Toloza et al. 2017). Although many types of research describe the effect dopant of boron, sulphur, nitrogen, and phosphorus and their utilization on CDs, none describe their effects used as candidate histamine detection in fish. In the present study, we improve the effectiveness of the dopant on CDs and investigate how the dopant can support the synergic emission of CDs on detecting histamine (Scheme 1). Several characterizations were prepared to evaluate the effectiveness of the doped CDs.

EXPERIMENTAL DETAILS

MATERIALS

The citric acid ($HOC(CO_2H)(CH_2CO_2H)_2$, 99,5%, Sigma-Aldrich), sulphuric acid (H_2SO_4, 97%, Sigma-Aldrich), boric acid (H_3BO_3, Sigma-Aldrich), nitric acid (HNO_3, Sigma-Aldrich), phosphoric acid (H_3PO_4, Sigma-Aldrich), sodium hydroxide (NaOH, Sigma-Aldrich), ethanol (C_2H_5OH, 96%, J.T. Baker), hydrochloride acid (HCl, 37%, Merck), histidine (Merck), sodium chloride (NaCl, Merck), magnesium chloride ($MgCl_2$, Merck), and potassium chloride (Merck).

SYNTHESIS OF CITRATE-CDs

The synthesis of citrate-CDs was approached by pyrolysis. Briefly, 0.0899 g of citrate acid was added to the vial and carbonated using a furnace for 2 h at 300 °C. The obtained citrate-CDs were brown blackies.

SYNTHESIS OF BORON-CDs (B-CDs)

Based on a similar approach, the synthesis of CDs doped with boron and sulphur was directed by pyrolysis. Approximately 0.0899 g of citrate acid and 0.0111 g of boric acid were added to the vial. Then, the mixture was carbonated using a furnace for 2 h at 300 °C until the color changed to brown blackies. The synthesis of B-CDs was finished.

SYNTHESIS OF SULPHUR-CDs (S-CDs)

The synthesized S-CDs were prepared by adding 0.0899 g of citrate acid, 99.9 µL H_2SO_4, and 50 µL NaOH in the vial. Then, the mixture was carbonated using a furnace for 2 h at 300 °C until the color changed to brown blackies and the B-CDs had been synthesized.

SYNTHESIS OF BORON SULPHUR-CDs (BS-CDs)

The BS-CDs were synthesized by adding 0.0899 g of citrate acid, 0.05 g boric acid, and 4.49 µL H_2SO_4 in the vial. Then, the 100 µL NaOH was added to the mixture solution and carbonated using a furnace for 2 h at 300 °C. The brown blackies BS-CDs have been finished synthesizing.

SYNTHESIS OF NITROGEN-CDs (N-CDs)

A pyrolysis approach prepared the synthesis of N-CDs. Briefly, 0.0899 g of citrate acid and 12.6 µL nitric acid were added to the vial and carbonated using a furnace for 2 h at 300 °C. The synthesis of B-CDs was finished with brown blackies in color.

SYNTHESIS OF PHOSPHOR-CDs (P-CDs)

The synthesis of P-CDs was prepared by adding 0.0899 g of citrate acid and 12.13 µL phosphoric acid in the vial. Then the mixture was carbonated using a furnace for 2 h at 300 °C until the color changed to brown blackies and the P-CDs had been synthesized.

SYNTHESIS OF NITROGEN PHOSPHOR-CDs (NP-CDs)

The BS-CDs were synthesized by adding 0.0899 g of citrate acid, 12.13 µL phosphoric acid, and 12.6 µL nitric

acid in a vial. Then, the mixture solution was carbonated using a furnace for 2 h at 300 ℃. The brown blackies BS-CDs have been finished synthesizing.

PREPARATION OF HISTAMINE SOLUTION

A histamine solution of 200 ppm was prepared by diluting 0.2 g in 100 mL of distilled water. Then, the histamine solution was dissolved into distilled water to achieve various concentrations of 1, 5, 25, 50, and 100 ppm.

CHARACTERIZATIONS

Several techniques are required to characterize the yields. UV-Vis spectra were recorded using a Shimadzu 1800 UV-Vis spectrophotometer (Shimadzu, Japan). Photoluminescence spectra were analyzed using a Spectrofluorometer LS 55 (Shimadzu, Jepang). Fourier transform infrared (FTIR) spectra were recorded using an infrared (IR) tracer-100 (Shimadzu, Japan). Dynamic light scattering (DLS) analysis was recorded using a Malvern analyzer. X-ray diffraction (XRD) diffractograms were recorded using an XRD Phillips. Atomic Force Microscope (AFM) images were recorded with AFM Park NX10, and RAMAN spectra were recorded with an RFT-6000 FT-RAMAN JASCO.

ANALYTICAL PERFORMANCE OF CDs

The detection limit (LOD) was determined using UV-Vis spectrophotometry, which relies on assessing absorbance values. The analysis involved varying concentrations of histamine. The Limit of Detection (LOD) analysis was performed by analyzing histamine samples with concentrations of 25, 50, and 100 ppm, each comprising 5 mL, and augmented with 100 µL of modified CDs. The results were graphed and analyzed to establish a calibration curve, providing information on the r value and linear equation. The LOD was calculated using Equation (1),

$$LoD = y_B + 3S_B \quad (1)$$

where SB represents the standard deviation, and yB is the blank response or intercept. All measurements were done in triplicate or three trials. The results were expressed as means of the standard deviation (SD).

CYTOTOXIC ASSAY

MTT assay was performed to test the toxicity using a 96-well microplate of each well will be filled with NP-CDs and BS-CDs samples with concentration variations of 500, 250, 125, 62.5, 31.2, 15.4, 7.5, and 3.75 µg/mL incubated with Hela cells for 24 h at 37 °C and 5% CO_2. After incubation, the dye 3-[4,5-dimethylthiazol-2-yl]2,5 diphenyl tetrazolium bromide (MTT) dye was added and then incubated at 37 °C for 4 h. Viability was then observed by optical density using an ELISA Multiplate Reader at a wavelength of 570 nm.

SELECTIVITY OF BS-CDS AND NP-CDs

Sample preparation was carried out by adding 100 ppm of histamine to 10 ppm of BS-CDs and NP-CDs, then adding ten ppm of interfering components such as histidine, NaCl, $MgCl_2$, and KCl.

RESULTS AND DISCUSSION

CDs were prepared through a simple pyrolysis approach (Aswandi et al. 2021). However, the formation of CD dopants at high heating causes dehydration and carbonization reactions, leading to structural rearrangements. The structural rearrangement process occurs through hydrogen bonding between citric acid and non-metal dopants H_3BO_3, H_2SO_4, HNO_3, and H_3PO_4. As shown in Scheme 1, the structural rearrangement process resulted in fluorescence, demonstrating the successful synthesis of heteroatom-doped CDs as a candidate for histamine detection. The B-CD, S-CD, BS-CD, N-CD, P-CD, and NP-CD solids are dark brown, while the undoped citric acid synthesis results in a black CD solid.

PHYSICOCHEMICAL PROPERTIES OF HETEROATOM DOPED CDs

To confirm the formation of CDs and heteroatom doped CDs, several characterizations such as UV-Vis, photoluminescence (PL), Fourier transform infrared (FTIR), atomic force microscopy (AFM), RAMAN, and X-ray diffraction (XRD) were conducted. UV-Vis analysis shows the maximum absorbance peaks of CDs, B-CDs, S-CDs, BS-CDs, N-CDs, P-CDs, and NP-CDs at 224, 226, 223, 224, 222, 222, and 222 nm, respectively. Meanwhile, the shoulder peak values for CDs-based samples ranged from 280 nm to 288 nm. The orbital

structures of Boron, Sulphur, Nitrogen, and Phosphorus allow UV absorption at wavelengths less than 300 nm for the π-π* transitions of the C=C bonds and the n-π* transitions of the C=O bonds (Aswandi et al. 2021; Liu et al. 2019). These phenomena show that doping with heteroatoms significantly changes the absorption spectra of CDs, as the doped elemental atoms are more bound to the surface or core of the CDs particles. In general, adding dopants reduces the intensity of shoulder peaks. Tauc plots of UV-Vis spectral data support the UV-Vis profile of CDs-based samples. The band gap value of CDs with different types of dopants ranges from 4.0771 to 5.3883 eV, where doped CDs have a higher band gap than undoped CDs (Figure 1(B)). The bandgap sequences of doped and undoped CDs are increased in the order of CDs < S-CDs < B-CDs < BS-CDs < N-CDs < P-CDs < NP-CDs. It proves that heat induction from pyrolysis can accelerate and support the effective carbonization of organic acids to form CDs. Furthermore, different band gaps on doped CDs are due to the dopant type of proposed elements. Compared to nitrogen and phosphorus combination dopant, which both perform n-type dopants, combination of boron and sulfur results in n-type combination on CDs and other graphene-like structures, even if boron dopants acts as a p-type originally. The hole is filled with sulphur, then the energy level moves to the conduction band and the band gap decreases, thereby causing a change in the nature of the carbon dot from p-type to n-type. This is expected to narrow the original band gap of CDs (Aswandi et al. 2021).

Another optical analytical test for doped CDs is photoluminescence (PL) analysis, as shown in Figure 1(C). Photoluminescence characterization has been demonstrated to determine the emission wavelengths produced by doped and undoped CDs, thus it can determine their fluorescence properties as well as their fluorescence intensity (Herman 2020). Based on the PL spectra analysis shows the highest excitation wavelength at 340 nm, with fluorescence emission of CDs increasing due to the addition of dopant compounds. B-CDs are among the doped CDs and undoped CDs compounds with the highest fluorescence emission intensity. It is confirmed by the results of quantum yield (QY) value calculations using the 6G-rhodamine standard. The order of the QY values of CDs, B-CDs, S-CDs, BS-CDs, N-CDs, P-CDs, and NP-CDs are 0.05%, 2.37%, 0.46%, 0.08%, 0.86%, 0.13%, and 1.72%, respectively. The resulting quantum yield values are shallow, which might be tormented by numerous elements, such as excessive carbonization temperature and lengthy synthesis time. If the temperature is too high, the molecules will differ, and the excited molecules' excess energy will be released to the solvent molecules (Zu et al. 2017). The highest QY value among the four analyzed samples was 2.37% for B-CD, suggesting that boron doping increases CD work function and fluorescence intensity. Boron is a p-type

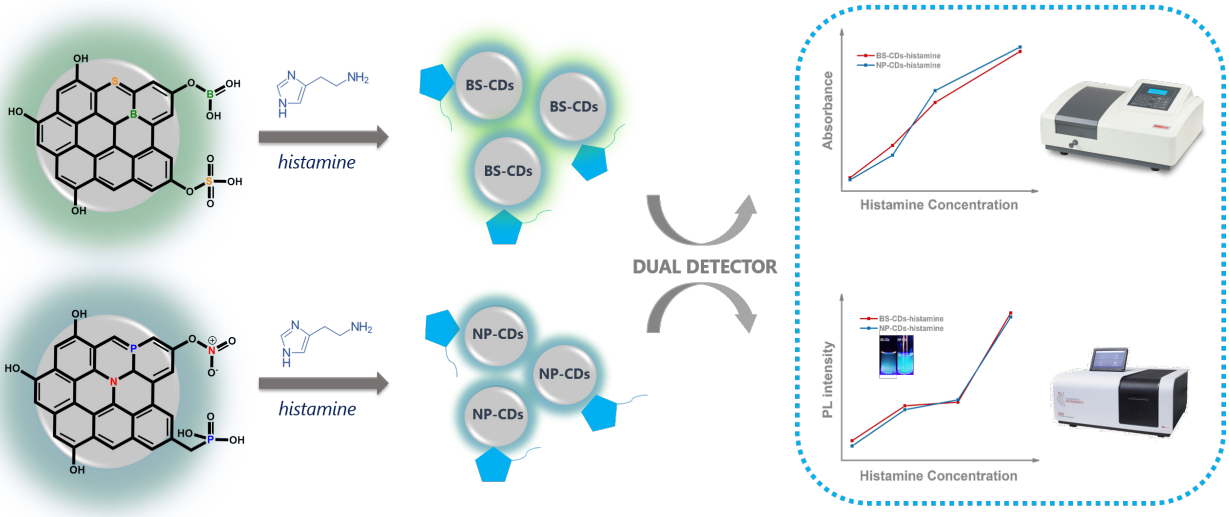

SCHEME 1. Schematic Illustration of CDs as a candidate for histamine detection

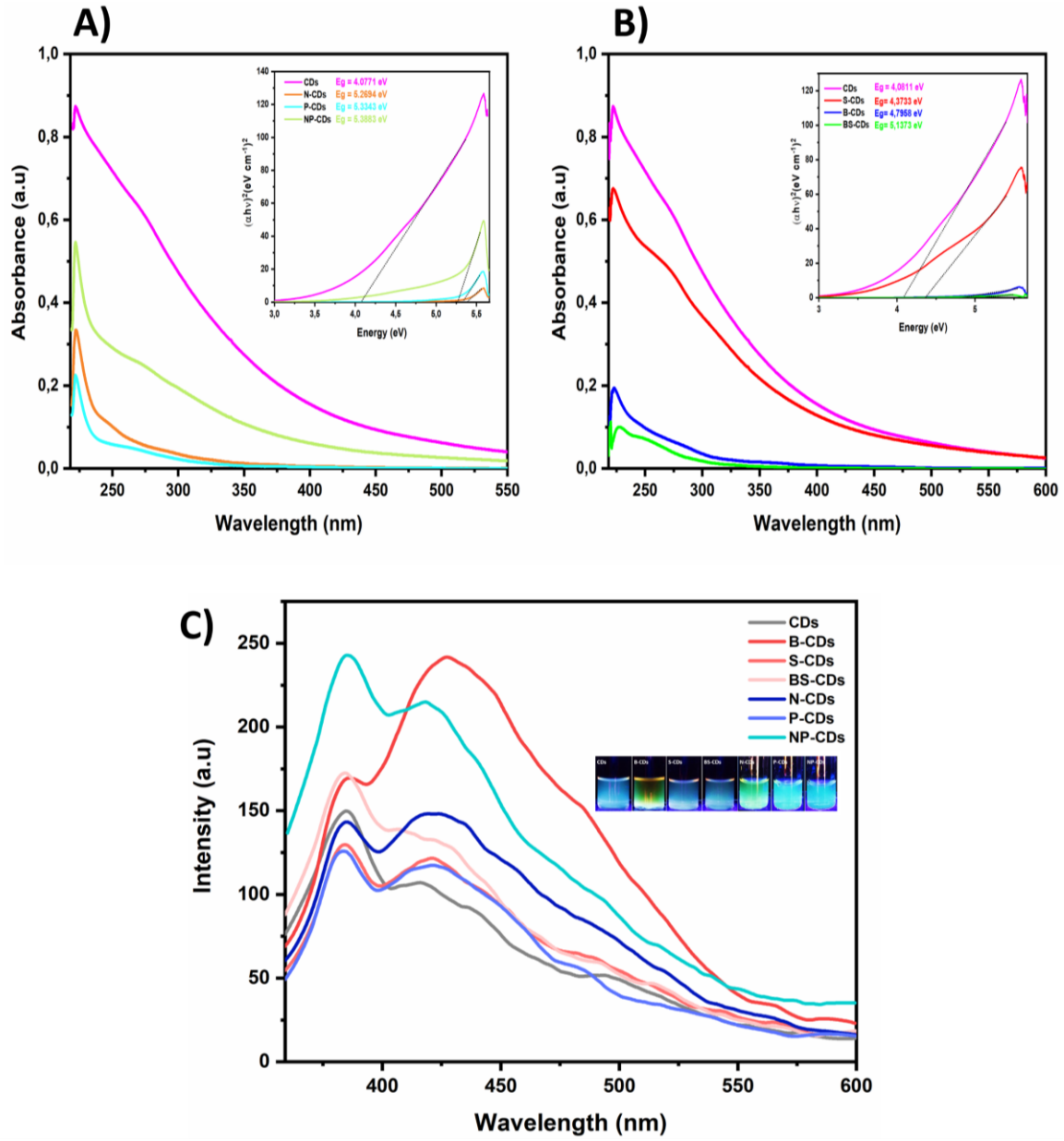

FIGURE 1. UV-Vis spectra and the band gap of A) CDs, N-CDs, P-CDs, NP-CDs; B) CDs-, B-CDs, S-CDs, BS-CDs, C) PL spectra of CDs, N-CDs, P-CDs, NP-CDs, CDs-, B-CDs, S-CDs, and BS-CDs

semiconductor that tends to increase the band gap as energy levels shift the valence band (Qu et al. 2021).

FTIR analysis was carried out to confirm the surface functional groups of doped CDs samples (2). The CDs spectrum shows different absorption bands at wavenumbers 3630 cm^{-1}, 2959 cm^{-1}, 1738 cm^{-1}, 1531 cm^{-1}, and 1207 cm^{-1} , which attributed to functional groups of O-H, C-H, C=O, C=C, and C-O, respectively. B-CDs spectra shows various absorption bands at wavenumbers 3223 cm^{-1}, 2959 cm^{-1}, 1767 cm^{-1}, 1531 cm^{-1}, 1447 cm^{-1}, and 1207 cm^{-1}, which corresponded to functional groups of O-H, C-H, C=O, C=C, B-O, and C-O, respectively. S-CDs sample show the presence of O-H, C-H, C=O, C=C, C-O, and S=C groups at absorption bands of 3630 cm^{-1}, 2959 cm^{-1}, 1738 cm^{-1}, 1531 cm^{-1}, 1207 cm^{-1}, and 1075 cm^{-1}, respectively. The successful doping process into

CDs containing the H_3BO_3 compound was also showed by CDs, where a stretching vibration at 1450 cm^{-1} indicates the presence of the B–O group, while S=C vibration give an FTIR signal at 1075 cm^{-1} (Atchudan et al. 2018; Bourlinos et al. 2015). BS-CDs with co-doping of H_3BO_3 and H_2SO_4 rendered O-H, C-H, C=O, C=C, B-O, C-O, S=C of functional group at wavenumbers 3223 cm^{-1}, 2959 cm^{-1}, 1767 cm^{-1}, 1531 cm^{-1}, 1447 cm^{-1}, 1207 cm^{-1}, and 1075 cm^{-1}, respectively (Figure 2(A)).

Figure 2(B) shows the FTIR profile of CDs, N-CDs, and P-CDs. The functional group of CDs, N-CDs and P-CDs show broad absorption bands at wavenumbers 3615, 3636, and 3614 cm^{-1} as the hydroxyl group, C-H group shows wavenumbers at 2970, 2959, and 2959 cm^{-1}, carbonyl C=O from citric acid at wavenumbers 1747, 1749, and 1713 cm^{-1}, and as C=C from benzene at wavenumbers 1556, 1526, and 1524 cm^{-1} are present in citrate compounds (Fahmi et al. 2021). The CDs, N-CDs, and P-CDs exhibit peaks at 1221, 1209, and 1020 cm^{-1}, respectively, indicating the presence of C-O functional groups in each sample. The FTIR co-dopants of NP-CDs spectrum render similar patterns as CDs, N-CDs, and P-CDs. NP-CDs has absorption bands at wavenumbers of 3620 cm^{-1}, 2952 cm^{-1}, 1754 cm^{-1}, 1522 cm^{-1}, and 1218 cm^{-1}, indicating the presence of O-H, C-H, C=O, C=C, and C-O, respectively. Both N-CDs and NP-CDs show the presence of C-N bonds at 1436 cm^{-1} and 1567 cm^{-1}, respectively. The similarity between P-CDs and NP-CDs has a wavenumber of 904 cm^{-1}, indicating the presence of P-O-C bonds (Gong et al. 2017).

AFM aims to describe three-dimensional shapes at atomic resolution, provide quantitative information about surface morphology, and determine the particle size distribution in two dimensions (De Oliveira et al. 2012). The results of the AFM analysis are shown in Figure 3(A). The particle shape of the BS-CDs particles is relatively uniform spheres with some variation in spherical diameter. The histograms in Figure 3(A) shows that the particle size distribution of both BS-CDs and NP-CDs is 2.6 nm. This data proves that the size distribution of the CDs with two dopants is 10 nm smaller than that of the undoped CDs. XRD analysis was performed to determine the crystal structures of BS-CDs and NP-CDs (Bunaciu, UdriŞTioiu & Aboul-Enein 2015). Based on Figure 3(B) most peaks formed originate from crystalline boron species in the CDs portion. The appearance of sharp peaks in the BS-CDs diffractogram evidence this. The broad peak in 2θ within 15°-50° indicates the amorphous character of boron-doped CDs, and the graphic structure (sp2) of CDs is confirmed based on reference JCPDS-26-1076 (Fahmi et al. 2020). BS-CDs have a high and sharp peak at 2θ = 27.8257° with an FWHM value is 0.0836, and the crystal diameter of BS-CDs is 1.785 nm. Meanwhile, the NP-CDs show one broad peak at 2θ 24.83°, indicating amorphous. The NP-CDs diffractogram is like graphene oxide with a peak at 24°. Amorphous graphite structures were also confirmed in JCPDS 74-2330 and JCPDS 41-1487, indicating the presence of C60 structures

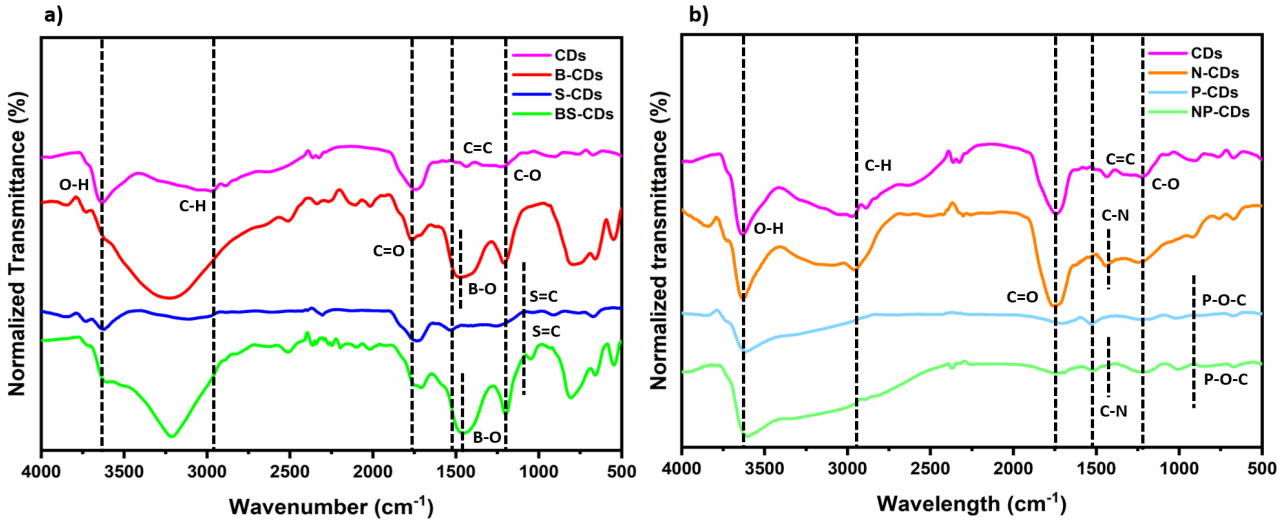

FIGURE 2. FTIR spectra of A) CDs-, B-CDs, S-CDs, BS-CDs and B) CDs, N-CDs, P-CDs, NP-CDs

(Nurul Ain et al. 2020; Tang et al. 2012). The NP-CDs peaks produced FWHM values of 0.090 and diameters of 1.64023 nm.

Analysis using Raman spectroscopy is required to support the analysis of CDs. Raman analysis observes molecular vibrations, rotations, and other low-frequency modes (Colthup 2012). Spectra for BS-CDs and NP-CDs analysis are shown in Figure 3(C). The BS-CDs spectrum explained that the D and G bands appeared at Raman shifts of 1386 cm^{-1} and 1586 cm^{-1}, respectively. D and G bands near 1330 cm^{-1} and 1586 cm^{-1} confirmed the presence of graphite (Gaddam et al. 2014). The NP-CDs spectra showed the presence of D and G bands at 1386 cm^{-1} and 1599 cm^{-1}, respectively. The D band peak is related to the irregularity of the carbon structure, and the sp3 carbon atom is obtained due to the amorphization of graphite during the oxidation process, while the G band peak shows the sp2 structure of graphite crystals. The intensity ratio of the D band (ID) and G band (IG) indicates different material properties of carbon. A smaller intensity ratio (ID/IG) between the D and G bands indicates better carbon dot formation and a more uniform surface state of the structure (Singh et al. 2019).

ANALYTICAL PERFORMANCE OF CDs

The limit of detection (LOD) is a limiting test parameter of a method's ability to detect the lowest amount of analyte. It showed that the concentration and absorbance of BS-CDs-histamine and NP-CDs-histamine were directly linear, as supported by increasing the intensity, as shown in Figure 4. The regression equations for both BS-CDs and NP-CDs were determined, with r values of 0.9747 and r of 0.9121, respectively. The equation for BS-CDs is $y = 0.0005x + 0.4$, and the equation for NP-CDs is $y = 0.0007x + 0.2375$. An r value approximating 1 indicates a linear correlation between concentration (x) and absorbance (y) (Nur 'Izzah et al. 2023). The

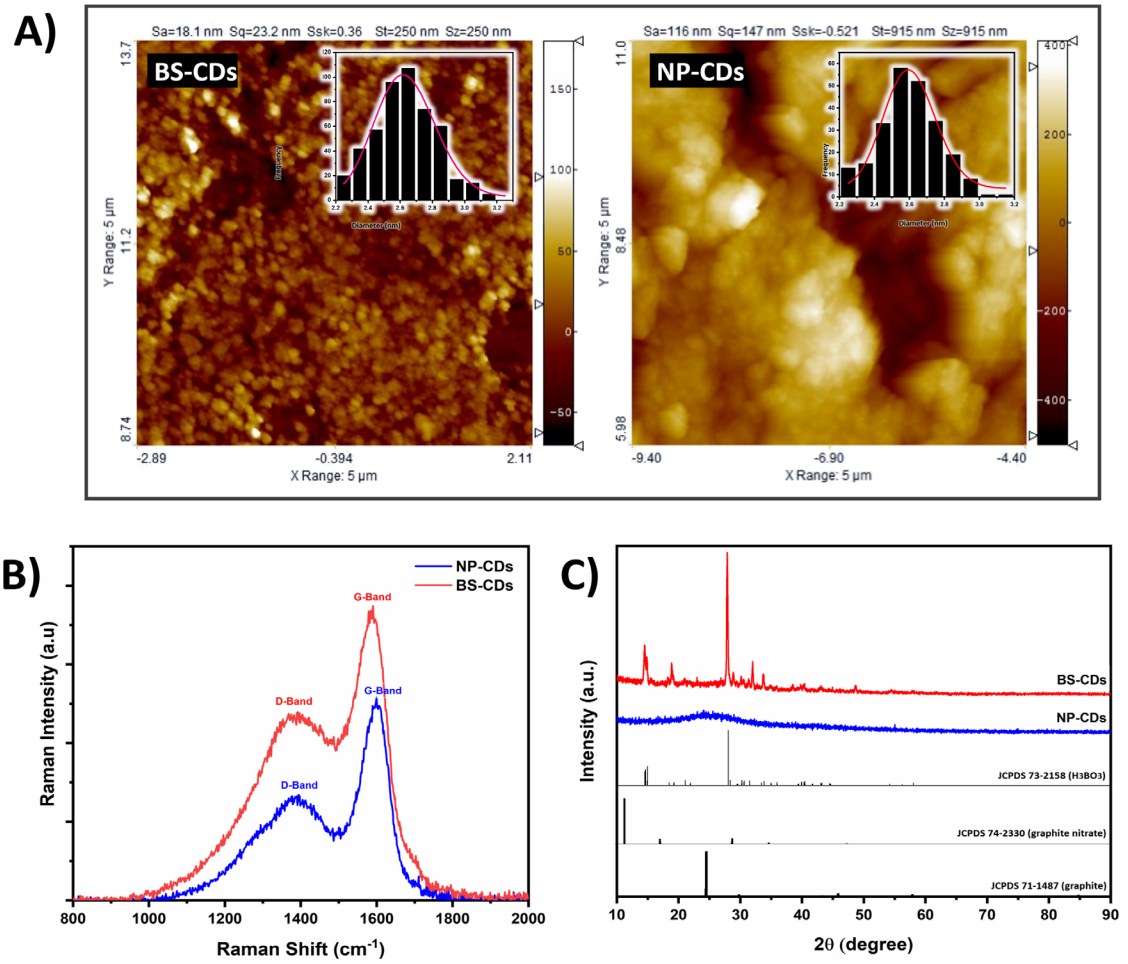

FIGURE 3. A) AFM image and histogram of BS-CDs and NP-CDs, B) XRD diffractogram of CDs, B-CDs and NP-CDs, and C) RAMAN spectra of NP-CDs and BS-CDs

calculated LOD for BS-CDs was 26.32 ppm, while it was 42.8 ppm for NP-CDs. LOD is a lower concentration that can be measured than the maximum histamine in fisheries, i.e., 50 ppm (DeBeer et al. 2021). So, it indicates that the BS-CDs and NP-CDs could detect histamine at minimum concentrations of 26.3 and 42.8 ppm.

SELECTIVITY OF BS-CDs AND NP-CDs

The selectivity test determines compounds or components that are selectively and carefully analyzed in the presence of other components in a sample matrix. Table 1 shows that the adjustment of interfering components to BS-CDs histamine and NP-CDs histamine affects selectivity at emission wavelength 420 nm. The fluorescence intensities of BS-CDs histamine and NP-CDs histamine decreased because of interfering components, indicating low selectivity of BS-CDs and NP-CDs for histamine.

CYTOTOXICITY ASSAY

An *in vitro* cytotoxicity test was conducted by MTT assay using HeLa cells. The formed formazan as purple complexes crystal coherently with a number of the living cell; this can be accessed on the state viability value of cells after being treated with BS-CDs and NP-CDs.

Figure 5 shows that the average viability generated was over 80%, demonstrating the low toxicity of BS-CDs and NP-CDs. Compounds with more than 80% cell viability are classified as non-toxic compounds, while 50-80% are classified as low-toxicity compounds (Singh et al. 2019; Nur Fatin Nabilah et al. 2021). Therefore, BS-CDs and NP-CDs are less toxic and can be safely used as sensors to detect the presence of histamine.

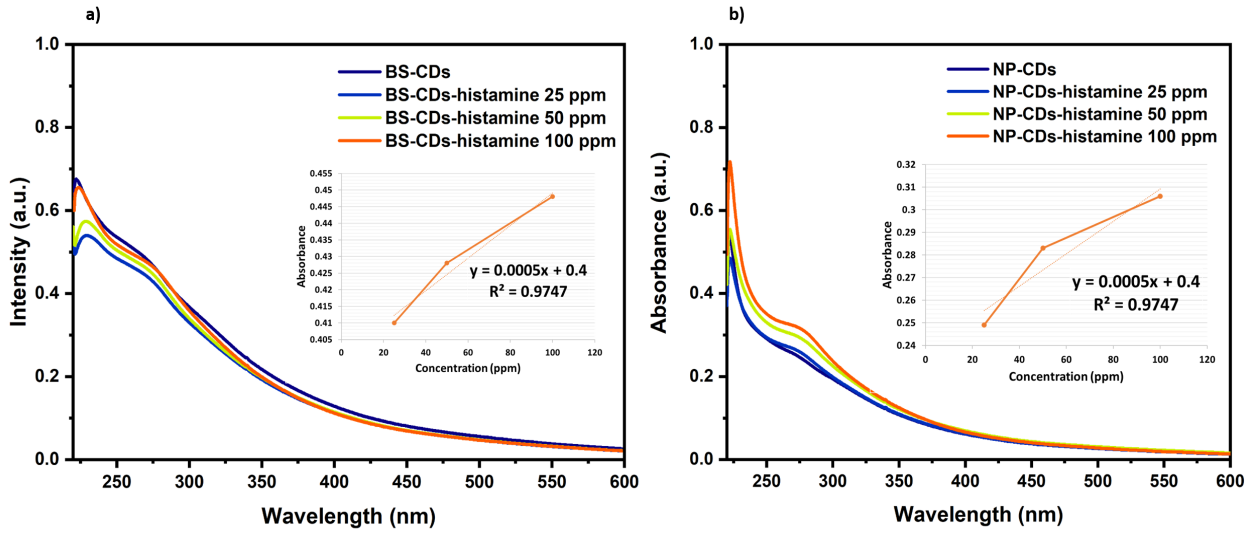

FIGURE 4. UV-Vis spectra and calibration curves of a) BS-CDs-histamine and b) NP-CDs-histamine in variation concentration

TABLE 1. The PL absorbance of matrix sample by adjustment of interfering NP-CDs-histamine and BS-CDs-histamine at 420 nm

Sample	BS-CDs-histamine	BS-CDs-histamine-histidine	BS-CDs-histamine-KCl	BS-CDs-histamine-NaCl	BS-CDs-histamine-$MgCl_2$	NP-CDs-histamine	NP-CDs-histamine-histidine	NP-CDs-histamine-KCl	NP-CDs-histamine-NaCl	**NP-CDs-histamine-$MgCl_2$**
Intensity (a.u.)	175.43	34.92	34.95	34.25	36.32	239.79	43.22	34.19	38.66	**40.45**

STABILIZATION OF CDs

Stability analyses of BS-CDs and NP-CDs against pH variation are intended to determine their stability under acidic and basic conditions. Therefore, a study was conducted for use as a histamine sensor in fish with optimum pH between 5-9 (Bi et al. 2020). Based on the UV-Vis and turbidity analysis in Figure 6, we conclude that BS-CDs and NP-CDs have high stability at pH 6-12 and are unstable in acidic conditions in the pH range of 3-5.

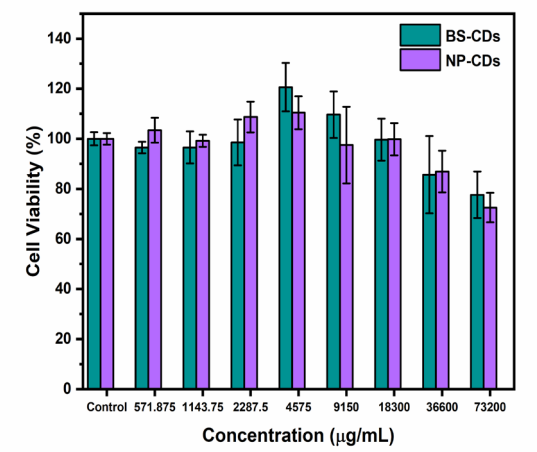

FIGURE 5. Viability cell of BS-CDs and NP-CDs

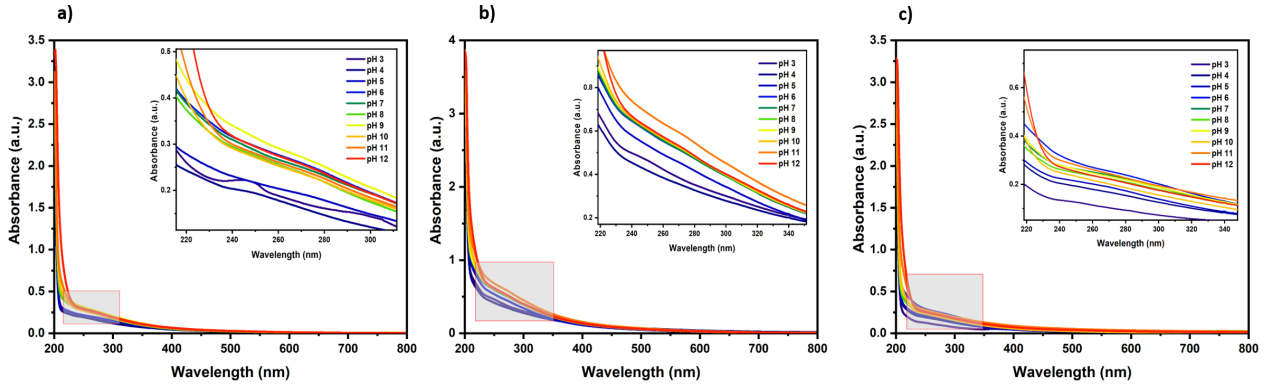

FIGURE 6. pH stabilization spectra of (a) CDs, (b) BS-CDs, and (c) NP-CDs

CONCLUSIONS

In summary, dual-dopant CDs have been successfully synthesized through a pyrolysis approach to producing BS-CDs and NP-CDs, resulting in uniform spheres crystals in diameters of both 2.6 nm. The formation of graphene-like structures on CDs was confirmed by Raman data response to the optical properties of the nanomaterial. The fluorescence intensity of BS-CDs and NP-CDs increased with the existence of histamine. Furthermore, the LOD showed that BS-CDs and NP-CDs could detect histamine at minimum concentrations of 26.3 and 42.8 ppm. This study opens further chances on modified CDs in other fields.

ACKNOWLEDGMENTS

Authors thank the RKI Republic Indonesia research scheme contract number 563/UN3.14/LT/2018.

REFERENCES

Arole, V.M. & Munde, S.V. 2014. Fabrication of nanomaterials by top-down and bottom-up approaches-an overview. *J. Mater. Sci.* 1: 89-93.

Aswandi Wibrianto, Siti Q. Khairunisa, Satya C.W. Sakti, Yatim L. Ni'Mah, Bambang Purwanto & Mochamad Z. Fahmi. 2021. Comparison of the effects of synthesis methods of B, N, S, and P-doped carbon dots with high photoluminescence properties on HeLa tumor cells. *RSC Advances* 11(2): 1098-1108.

Atchudan, R., Jebakumar Immanuel Edison, T.N., Perumal, S., Karthik, N., Karthikeyan, D., Shanmugam, M. & Lee, Y.R. 2018. Concurrent synthesis of nitrogen-doped carbon dots for cell imaging and ZnO@nitrogen-doped carbon sheets for photocatalytic degradation of methylene blue. *Journal of Photochemistry and Photobiology A: Chemistry* 350: 75-85.

Baker, S.N. & Baker, G.A. 2010. Luminescent carbon nanodots: Emergent nanolights. *Angewandte Chemie International Edition* 49(38): 6726-6744.

Bi, J., Tian, C., Zhang, G-L., Hao, H. & Hou, H-M. 2020. Detection of histamine based on gold nanoparticles with dual sensor system of colorimetric and fluorescence. *Foods* 9(3): 1-10.

Bourlinos, A.B., Trivizas, G., Karakassides, M.A., Baikousi, M., Kouloumpis, A., Gournis, D., Bakandritsos, A., Hola, K., Kozak, O., Zboril, R., Papagiannouli, I., Aloukos, P. & Couris, S. 2015. Green and simple route toward boron doped carbon dots with significantly enhanced non-linear optical properties. *Carbon* 83: 173-179.

Bunaciu, A.A., UdriŞTioiu, E.G. & Aboul-Enein, H.Y. 2015. X-ray diffraction: Instrumentation and applications. *Critical Reviews in Analytical Chemistry* 45(4): 289-299.

Chatterjee, M., Nath, P., Kadian, S., Kumar, A., Kumar, V., Roy, P., Manik, G. & Satapathi, S. 2022. Highly sensitive and selective detection of dopamine with boron and sulfur co-doped graphene quantum dots. *Scientific Reports* 12(1): 9061.

Colthup, N. 2012. *Introduction to Infrared and Raman Spectroscopy*. Elsevier.

De Oliveira, R.R.L., Albuquerque, D.A.C., Cruz, T.G.S., Yamaji, F.M. & Leite, F.L. 2012. Measurement of the nanoscale roughness by atomic force microscopy: Basic principles and applications. In *Atomic Force Microscopy-Imaging, Measuring and Manipulating Surfaces at the Atomic Scale*, edited by Bellitto, V. InTech. http://www.intechopen.com/books/atomic-force-microscopyimaging-measuring-and-manipulating-surfaces-at-the-atomic-scale/measurement-of-the-nanoscaleroughness-by-atomic-force-microscopy-basic-principles-and-applications

DeBeer, J., Bell, J.W., Nolte, F., Arcieri, J. & Correa, G. 2021. Histamine limits by country: A survey and review. *Journal of Food Protection* 84(9): 1610-1628.

Fahmi, M.Z., Sholihah, N.F., Wibrianto, A., Sakti, S.C.W., Firdaus, F. & Chang, J-Y. 2021. Simple and fast design of folic acid-based carbon dots as theranostic agent and its drug release aspect. *Materials Chemistry and Physics* 267: 124596.

Fahmi, M.Z., Prasetya, R.A., Dzikri, M.F., Sakti, S.C.W. & Yuliarto, B. 2020. $MnFe_2O_4$ nanoparticles/cellulose acetate composite nanofiber for controllable release of naproxen. *Materials Chemistry and Physics* 250: 123055.

Gaddam, R.R., Vasudevan, D., Narayan, R. & Raju, K. 2014. Controllable synthesis of biosourced blue-green fluorescent carbon dots from camphor for the detection of heavy metal ions in water. *RSC Advances* 4(100): 57137-57143.

Gong, X., Liu, Y., Yang, Z., Shuang, S., Zhang, Z. & Dong, C. 2017. An "on-off-on" fluorescent nanoprobe for recognition of chromium (VI) and ascorbic acid based on phosphorus/nitrogen dual-doped carbon quantum dot. *Analytica Chimica Acta* 968: 85-96.

Gunjal, D.B., Nille, O.S., Naik, V.M., Shejwal, R.V., Kolekar, G.B. & Gore, A.H. 2023. Chapter 14 - Heteroatom/metal ion-doped carbon dots for sensing applications. In *Carbon Dots in Analytical Chemistry*, edited by Kailasa, S.K. & Hussain, C.M. Elsevier. pp. 181-197.

Herman, B. 2020. *Fluorescence Microscopy*. Garland Science.

Hola, K., Zhang, Y., Wang, Y., Giannelis, E.P., Zboril, R. & Rogach, A.L. 2014. Carbon dots - Emerging light emitters for bioimaging, cancer therapy and optoelectronics. *Nano Today* 9(5): 590-603.

Huang, C., Wang, S., Zhao, W., Zong, C., Liang, A., Zhang, Q. & Liu, X. 2017. Visual and photometric determination of histamine using unmodified gold nanoparticles. *Microchimica Acta* 184(7): 2249-2254.

Kim, Y. & Chang, J.Y. 2016. Fabrication of a fluorescent sensor by organogelation: CdSe/ZnS quantum dots embedded molecularly imprinted organogel nanofibers. *Sensors and Actuators B: Chemical* 234: 122-129.

Li, L., Yu, B. & You, T. 2015. Nitrogen and sulfur co-doped carbon dots for highly selective and sensitive detection of Hg (II) ions. *Biosensors and Bioelectronics* 74: 263-269.

Liu, H., Ding, J., Zhang, K. & Ding, L. 2019. Construction of biomass carbon dots based fluorescence sensors and their applications in chemical and biological analysis. *TrAC Trends in Analytical Chemistry* 118: 315-337.

Mandawala, C., Chebbi, I., Durand-Dubief, M., Le Fèvre, R., Hamdous, Y., Guyot, F. & Alphandéry, E. 2017. Biocompatible and stable magnetosome minerals coated with poly-l-lysine, citric acid, oleic acid, and carboxy-methyl-dextran for application in the magnetic hyperthermia treatment of tumors. *Journal of Materials Chemistry B* 5(36): 7644-7660.

Mirsadoughi, E., Nemati, F., Oroojalian, F. & Hosseini, M. 2022. Turn –on FRET-based cysteine sensor by sulfur-doped carbon dots and Au nanoparticles decorated WS2 nanosheet. *Spectrochimica Acta Part A: Molecular and Biomolecular Spectroscopy* 272: 120903.

Munusamy, S., Mandlimath, T.R., Swetha, P., Al-Sehemi, A.G., Pannipara, M., Koppala, S., Shanmugam, P., Boonyuen, S., Pothu, R. & Boddula, R. 2023. Nitrogen-doped carbon dots: Recent developments in its fluorescent sensor applications. *Environmental Research* 231: 116046.

Nurul Ain Huzaifah, Nordin Sabli, Kok Kuan Ying, Nur Ubaidah Saidin & Hikmat S. Hilal. 2020. Enhancement of characteristics of nitrogen-doped graphene composite materials prepared by ball milling of graphite with melamine: Effect of milling speed and material ratios. *Sains Malaysiana* 49(7): 1745-1754.

Nur Fatin Nabilah Mohd Sahardi, Faizul Jaafar, Siti Nor Asyikin Zakaria, Jen Kit Tan, Mariam Firdhaus Mad Nordin & Suzana Makpol. 2021. Comparison of the antioxidant activity of Malaysian ginger (*Zingiber officinale* Roscoe) extracts with that of selected natural products and its effect on the viability of myoblast cells in culture. *Sains Malaysiana* 50 (5): 1445-1456.

Nur 'Izzah binti Ahmad Juanda, Noorashikin Md Saleh, Nor Yuliana Yuhana, Saliza Asman & Farhanini Yusoff. 2023. Analysis of methylphenol concentration in Selangor Rivers, Malaysia using solid phase extraction technique coupled with UV-Vis spectroscopy. *Sains Malaysiana* 52(5): 1453-1468.

Preethi, M., Viswanathan, C. & Ponpandian, N. 2022. Fluorescence quenching mechanism of P-doped carbon quantum dots as fluorescent sensor for Cu^{2+} ions. *Colloids and Surfaces A: Physicochemical and Engineering Aspects* 653: 129942.

Qu, Y., Ding, J., Fu, H., Chen, H. & Peng, J. 2021. Investigation on tunable electronic properties of semiconducting graphene induced by boron and sulfur doping. *Applied Surface Science* 542: 148763.

Schneider, J., Reckmeier, C.J., Xiong, Y., von Seckendorff, M., Susha, A.S., Kasák, P. & Rogach, A.L. 2017. Molecular fluorescence in citric acid-based carbon dots. *The Journal of Physical Chemistry C* 121(3): 2014-2022.

Singh, A.K., Singh, V.K., Singh, M., Singh, P., Khadim, S.R., Singh, U., Koch, B., Hasan, S.H. & Asthana, R.K. 2019. One pot hydrothermal synthesis of fluorescent NP-carbon dots derived from *Dunaliella salina* biomass and its application in on-off sensing of Hg (II), Cr (VI) and live cell imaging. *Journal of Photochemistry and Photobiology A: Chemistry* 376: 63-72.

Tang, L., Ji, R., Cao, X., Lin, J., Jiang, H., Li, X., Teng, K.S., Luk, C.M., Zeng, S. & Hao, J. 2012. Deep ultraviolet photoluminescence of water-soluble self-passivated graphene quantum dots. *ACS Nano* 6(6): 5102-5110.

Ternero-Hidalgo, J.J., Rosas, J.M., Palomo, J., Valero-Romero, M.J., Rodríguez-Mirasol, J. & Cordero, T. 2016. Functionalization of activated carbons by HNO_3 treatment: Influence of phosphorus surface groups. *Carbon* 101: 409-419.

Toloza, C.A.T., Khan, S., Silva, R.L.D., Romani, E.C., Larrude, D.G., Louro, S.R.W., Freire Júnior, F.L. & Aucelio, R.Q. 2017. Photoluminescence suppression effect caused by histamine on amino-functionalized graphene quantum dots with the mediation of Fe^{3+}, Cu^{2+}, Eu^{3+}: Application in the analysis of spoiled tuna fish. *Microchemical Journal* 133: 448-459.

Wang, B., Cai, H., Waterhouse, G.I.N., Qu, X., Yang, B. & Lu, S. 2022. Carbon dots in bioimaging, biosensing and therapeutics: A comprehensive review. *Small Science* 2(6): 2200012.

Wang, F., Hao, Q., Zhang, Y., Xu, Y. & Lei, W. 2016. Fluorescence quenchometric method for determination of ferric ion using boron-doped carbon dots. *Microchimica Acta* 183: 273-279.

Wang, Y. & Hu, A. 2014. Carbon quantum dots: Synthesis, properties and applications. *Journal of Materials Chemistry C* 2(34): 6921-6939.

Xu, Q., Liu, Y., Gao, C., Wei, J., Zhou, H., Chen, Y., Dong, C., Sreeprasad, T.S., Li, N. & Xia, Z. 2015. Synthesis, mechanistic investigation, and application of photoluminescent sulfur and nitrogen co-doped carbon dots. *Journal of Materials Chemistry C* 3(38): 9885-9893.

Yadav, S., Nair, S.S., Sai, V.V.R. & Satija, J. 2019. Nanomaterials based optical and electrochemical sensing of histamine: Progress and perspectives. *Food Research International* 119: 99-109.

Zang, Z., Zeng, X., Wang, M., Hu, W., Liu, C. & Tang, X. 2017. Tunable photoluminescence of water-soluble AgInZnS–graphene oxide (GO) nanocomposites and their application *in-vivo* bioimaging. *Sensors and Actuators B: Chemical* 252: 1179-1186.

Zhang, D., Wang, Y., Xie, J., Geng, W. & Liu, H. 2020. Ionic-liquid-stabilized fluorescent probe based on S-doped carbon dot-embedded covalent-organic frameworks for determination of histamine. *Microchimica Acta* 187: 1-9.

Zhou, M., Zhou, Z., Gong, A., Zhang, Y. & Li, Q. 2015. Synthesis of highly photoluminescent carbon dots via citric acid and Tris for iron (III) ions sensors and bioimaging. *Talanta* 143: 107-113.

Zu, F., Yan, F., Bai, Z., Xu, J., Wang, Y., Huang, Y. & Zhou, X. 2017. The quenching of the fluorescence of carbon dots: A review on mechanisms and applications. *Microchimica Acta* 184: 1899-1914.

Zuo, P., Lu, X., Sun, Z., Guo, Y. & He, H. 2016. A review on syntheses, properties, characterization and bioanalytical applications of fluorescent carbon dots. *Microchimica Acta* 183: 519-542.

*Corresponding author; email: m.zakki.fahmi@fst.unair.ac.id